Efficient Polymer Solar Cells Based on New Random Copolymers with Porphyrin-Incorporated Side Chains

Zhixin Liu,[§] Zhuohao Huang,[§] Yuzhuo Chen,[§]Tao Xu, Hao Yu, Xia Guo, Lei Yan[*], Maojie Zhang[*], Wai-Yeung Wong[*], and Xingzhu Wang[*]

Z. Liu, Z. Huang, Y. Chen, T. Xu, Dr. L. Yan, Prof. X. Wang
College of Chemistry and School of Physics and Optoelectronics
Xiangtan University
Xiangtan 411105, P.R. China.
E-mail: xz_wang@hotmail.com, yanlei@xtu.edu.cn
Prof. X. Guo, Prof. M. Zhang
State and Local Joint Engineering Laboratory for Novel Functional Polymeric Materials, Laboratory of Advanced Optoelectronic Materials, College of Chemistry, Chemical Engineering and Materials Science
Soochow University
Suzhou 215123, P.R. China
E-mail: mjzhang@suda.edu.cn
Prof. W.-Y. Wong
Department of Applied Biology and Chemical Technology
The Hong Kong Polytechnic University (PolyU)
Hung Hom, Hong Kong, P.R. China and
PolyU Shenzhen Research Institute,
Shenzhen 518057, P.R. China
E-mail: wai-yeung.wong@polyu.edu.hk

Two new wide bandgap block copolymers (PL1 and PL2) with porphyrin-incorporated side chains have been designed and used as electron donors for solution-processed bulk heterojunction (BHJ) polymer solar cells. The photophysical, electrochemical and photovoltaic properties, charge transport mobility and film morphology of these two block copolymers were investigated. Detailed investigations revealed that the different alkyl groups and electron-withdrawing substituents on the porphyrin pendant units have significant influence on the polymer solubility, absorption energy level, band gap and charge separation in the bulk-heterojunction thin films, and thus the overall photovoltaic performances. Organic photovoltaic devices derived from these copolymers and $PC_{71}BM$ acceptor showed the best

power conversion efficiencies (PCE) of 5.83% and 7.14%, respectively. These results show that the inclusion of a certain proportion of side chain porphyrin group as a pendant in the traditional D-A type polymer can broaden the molecular absorption range and become a full-color absorbing molecule. The size of the porphyrin pendant also has an obvious effect on the properties of the molecule.

1. Introduction

Organic solar cells (OSCs) consisting of various building blocks are attracting considerable attention because of their light-weight, high flexibility and easy processing as well as the potential to tune the optical, mechanical, and electrical properties.[1-5] Based on these advantages, OSCs have achieved significant advances recently.[6-9] At present, the energy conversion efficiency (PCEs) of the single-junction fullerene polymer solar cells based on conjugated polymers as the donor has exceeded 16%.[10-15] The photovoltaic properties of OSCs based on donors containing porphyrin rings and their derivatives are impressive,[16] and they have been used in dye-sensitized solar cells (DSSCs) for a long time.[17-19] However, porphyrin-based polymers or small molecules (SM) contribute relatively less to BHJ OSCs. At the same time, porphyrin and its derivatives have excellent electrochemical properties and thermal stability. It has a planar largely π-conjugated structure, and the π-π accumulation between extensively conjugated π bonds gives it a high electron mobility along the stacked direction.[20-23] While the performance barriers of inferior solubility, distasteful aggregation, insufficient exciton diffusion distance and bad charge mobility need to be solved,[24-26] we envision that porphyrin-containing polymers will play a more significant role in BHJ OSCs through a wise configurational design.

At present, the optical absorption range of organic semiconductor is often too narrow to achieve panchromatic absorption which is crucial for conceiving high efficiency.[27] To this end, the third component has been introduced into the traditional D-A conjugated polymer

which improves the properties of the polymer, such as energy level, band gap, and the correlation between the current and voltage balance to optimize the molecular structure for high device performance.[28-30] The ternary random copolymerization could be an effective strategy to realize the excellent solubility and low degree of aggregation of the corresponding polymers and suitable molecular orbital energy levels and improved light harvesting capability.[31, 32]

Herein, we synthesized two novel block copolymers (**PL1** and **PL2**) (**Figure 1**) by incorporating porphyrin pendant units as a complementary light-harvesting unit in a conventional D-A polymer, and obtained two new panchromatic absorbers. The effects of different porphyrin pendants on the spectral absorption, charge transfer, morphology and photovoltaic properties were investigated. The two polymers consist of thienyl-porphyrins (compounds Por1 and Por2, respectively), bis(trimethyltin) BDT monomer and the dibromo TT species. All the conditions and steps for the synthesis of these two polymers are shown in **Scheme 1**. The high solubility of Zn-porphyrin allows the copolymers to be easily fabricated into devices.

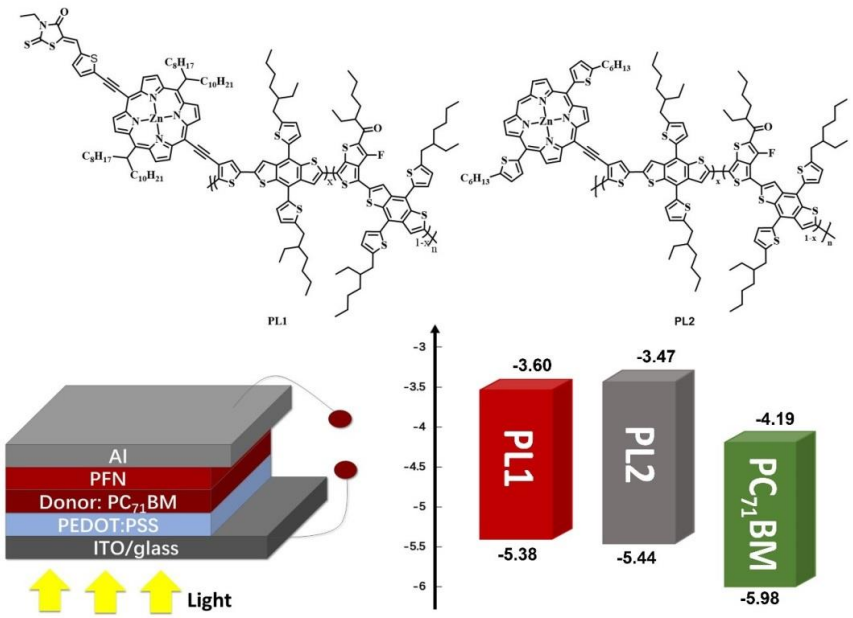

Figure 1. Molecular structures of **PL1** and **PL2**, the device structure, energy level diagram of **PL1**, **PL2** and $PC_{71}BM$.

2. Experimental Section

2.1 Materials and synthesis

All chemicals and solvents were purchased from Suna Tech Inc., Aldrich, Alfa Aesar. and were used as received unless otherwise noted. (4,8-Bis(5-octylthiophen-2- yl)benzo[1,2–b:4,5-b']dithiophene-2,6-diyl)bis(trimethylstannane) (BDT) and 2- ethylhexyl-4,6–dibromo-3-fluorothieno[3,4-b]thiophene–2-carboxylate (TT) were purchased from Suna Tech Inc. All air and water sensitive reactions were performed under an argon atmosphere. Toluene and tetrahydrofuran were purified according to the literature method prior to use. The compounds **4** and **7** were synthesized according to the literature.[33] The synthetic routes of **PL1** and **PL2** are shown in **Scheme 1** and their chemical compositions were characterized by ^{1}H NMR and ^{13}C NMR spectroscopy and MALDI-TOF mass spectrometry.

2.1.1. Synthesis of compound **2**

In a 500-mL flask, 2,5-dibromo-3-iodothiophene (2 g, 5.44 mmol) was dissolved in THF (30 mL) and Et_3N (6 mL) and the solution was bubbled with argon for 30 min. After that, trimethylsilylacetylene (3.86 mL, 27.2 mmol), $PdCl_2(PPh_3)_2$ (190 mg, 0.27 mmol), CuI (51 mg, 0.27 mmol) and PPh_3 were added to the solution under a nitrogen flow. The reaction mixture was heated to 60 ^{o}C for 8 h. After cooling to 20 ^{o}C, removal of the solvent *in vacuo* followed by column chromatography (SiO_2, hexane) yielded the desired compound 1 (1.56 g, 84%) as a yellow oil.

2.1.2. Synthesis of compound **3**

To a 200-mL flask, **2** (1.56 g, 4.60 mmol), K_2CO_3 (1.91 g, 13.8 mmol), and methanol (30 mL) were added, and the mixture was stirred at 20 ^{o}C for 3 h. The mixture was diluted with dichloromethane and the organic phase was washed three times with water. After drying over Na_2SO_4, the solution was filtered. Removal of the solvent *in vacuo* and column

chromatography (SiO_2, hexane) yielded the desired compound **3** (1.17 g, 95%) as a scarlet solid. ^{1}H NMR (400 MHz, $CDCl_3$, δ): 3.30 (s, 1 H), 6.96 ppm (s, 1H). ^{13}C NMR (100 MHz, $CDCl_3$, δ): 76.12, 81.68, 110.96, 117.08, 123.97, 132.22 ppm.

2.1.3. Synthesis of compound **5**

In a 500-mL flask, **4** (500 mg, 0.47 mmol) and 5-ethynylthiophene-2-carbaldehyde (63.9 mg, 0.47 mmol) were dissolved in THF (15 mL) and Et_3N (3 mL) and the solution was bubbled with argon for 30 min. After that, $Pd(PPh_3)_4$ (35 mg, 0.03 mmol) and CuI (5.7 mg, 0.03 mmol) were added to the solution under a nitrogen flow. The solution was refluxed for 12 h under nitrogen. The solvent was removed under vacuum, and the solid residue was purified by preparative thin layer chromatography using a $CHCl_3$/hexane (2:1) as eluent. Recrystallization from $CHCl_3$/methanol gave **5** as a purple solid. ^{1}H NMR (400 MHz, $CDCl_3$, δ): 9.97 (s, 1H), 9.84-9.49 (m, 6H), 9.27 (m, 2H), 7.85 (d, 2H), 7.69 (d, 2H), 5.22 (d, J = 32.3 Hz, 2H), 2.96 (m, 4H), 2.72 (m, 4H), 1.57 (m, 5H), 1.41-0.91 (m, 51H), 0.87-0.65 (m, 12H). MALDI-TOF MS (m/z): calcd for $C_{65}H_{89}BrN_4OSZn$: 1119.8, found: 1120.257.

2.1.4. Synthesis of compound **6**

In a 500-mL flask, **5** (300 mg, 0.27 mmol) and **2** (71.2 mg,0.27mmol) were dissolved in THF (15 mL) and Et_3N (3 mL) and the solution was bubbled with argon for 30 min. After that, $Pd(PPh_3)_4$ (35 mg, 0.03 mmol) and CuI (5.7 mg, 0.03 mmol) were added to the solution under a nitrogen flow. The solution was refluxed for 12 h under nitrogen. The solvent was removed under vacuum, and the solid residue was purified by preparative thin layer chromatography using a $CHCl_3$/hexane (3:1) as eluent. Recrystallization from $CHCl_3$/methanol gave **6** as a purple solid. ^{1}H NMR (400 MHz, $CDCl_3$, δ): 10.42 (s, 2H), 9.74 (m, 8H), 8.23 (d, 1H), 7.51 (s, 1H), 7.11 (d, 1H), 5.26 m, 2H), 3.03 (m, 4H), 2.78 (m, 4H), 1.10 (m, 48H), 0.93 -0.81 (m, 16H), 0.77 (m, 12H). ^{13}C NMR (100 MHz, $CDCl_3$, δ): 182.36, 152.23, 152.10, 149.78, 149.35, 149.06, 148.42, 148.14, 147.87, 136.61, 135.71, 135.47, 135.22, 134.86, 134.39, 134.02,

133.87, 132.15, 131.58, 130.93, 130.65, 130.34, 130.04, 129.91, 129.69, 128.63, 128.54, 127.76, 127.09, 123.15, 122.90, 122.65, 111.34, 98.16, 88.56, 88.41, 47.02, 42.50, 31.82, 31.76, 29.95, 29.73, 29.50, 29.47, 29.21, 29.18, 22.62, 22.54, 14.07, 14.05. MALDI-TOF MS (m/z): calcd for $C_{71}H_{90}Br_2N_4OS_2Zn$: 1304.84, found: 1304.030.

2.1.5. Synthesis of compound **Por1**

To a solution of **6** (200 mg, 0.15 mmol) in $CHCl_3$ (20 mL), two drops of piperidine and 3-ethylrhodanine (228.3 mg, 1.370 mmol) were added, and the resulting solution was refluxed for 12 h under argon. The reaction was quenched with water (30 mL) and extracted with $CHCl_3$ (3 × 20 mL). The organic layer was dried over Na_2SO_4 and evaporated to dryness. The solid residue was purified first on a silica gel column and second by preparative thin layer chromatography using $CHCl_3$ as eluent. Further recrystallization from hexane and $CHCl_3$ mixed solvent for five times afforded the target compound **Por1** as a black solid. ^{1}H NMR (400 MHz, $CDCl_3$, δ): 9.83-9.44 (m, 8H), 8.22 (d, 1H), 7.76 (s, 1H), 7.25 (s, 1H), 7.17 (d, 1H), 5.20 (s, 2H), 4.24 (q, *J* = 7.1 Hz, 2H), 2.96 (d, *J* = 9.8 Hz, 4H), 2.72 (s, 4H), 2.57 (s, 3H), 1.51 (s, 4H), 1.34 (t, *J* = 7.1 Hz, 7H), 1.25-1.20 (m, 3H), 1.18-0.96 (m, 43H), 0.81-0.68 (m, 12H). MALDI-TOF MS (m/z): calcd for $C_{76}H_{95}Br_2N_5OS_4Zn$: 1448.06, found: 1447.192.

2.1.6. Synthesis of compound **8**

To a two-neck round flask N-iodosuccinimide (277.7 mg, 1.24 mmol) was added to compound **7** (800 mg,1.24 mmol) in 100 mL chloroform under nitrogen. The mixture was stirred at room temperature for 0.5 h, and quenched with 100 mL of methanol. After the filtration, the solid was dissolved in 100 mL chloroform and 0.5 mL of pyridine, followed by the addition of $Zn(OAc)_2 \cdot 2H_2O$ (664 mg, 3 mmol) in methanol (10 mL). The reaction mixture was stirred overnight at room temperature. The solvents were removed, and the residue was washed with ethanol three times and then purified by column chromatography using

$CHCl_3$/hexane (3:1) as the eluent. A purple solid was obtained after the recrystallization from DCM/ethanol.

2.1.7. Synthesis of compound **Por2**

In a 500-mL flask, **3** (500 mg, 0.60 mmol) and **2** (159.7 mg,0.60 mmol) were dissolved in THF (15 mL) Et_3N (3 mL) and the solution was bubbled with argon for 30 min. After that, $Pd(PPh_3)_4$ (35 mg, 0.03 mmol) and CuI (5.7 mg, 0.03 mmol) were added to the solution under a nitrogen flow. The solution was refluxed for 12 h under nitrogen. The solvent was removed under vacuum, and the solid residue was purified by preparative thin layer chromatography using a $CHCl_3$/hexane (3:1) as eluent. Recrystallization from $CHCl_3$/methanol gave **Por2** as a purple solid. ^{1}H NMR (400 MHz, $CDCl_3$, δ): 9.98 (s, 1 H), 9.71 (s, 1 H), 9.33 (s, 1 H), 9.20 (m, 12H), 9.12 (m, 12H), 9.06 (m, 12H), 7.69 (m, 12H), 7.22 (m, 12H), 3.23(m, 12H), 2.05 (m, 12H), 1.68 (m, 12H), 1.07-1.38 (m, 12H). ^{13}C NMR (100 MHz, $CDCl_3$, δ): 150.58, 149.92, 148.66, 148.46, 147.43, 140.05, 133.72, 133.21, 132.00, 131.73, 131.29, 130.92, 125.52, 123.45, 115.72, 112.10, 111.40, 111.00, 105.60, 103.33, 89.64, 89.40, 77.39, 77.07, 76.76, 31.96, 30.56, 29.77, 29.26, 22.86, 14.35.ppm. MALDI-TOF MS (m/z): calcd for $C_{46}H_{40}Br_2N_4S_3Zn$: 970.2220; found, 971.7870.

2.1.8. Synthesis of **PL1**

To an eggplant type reaction bottle containing compound **3** (8.6 mg, 0.01 mmol), BDT (100 mg, 0.111 mmol) and TT (48.4 mg, 0.110 mmol) in a mixture of degassed toluene (2.4 mL) and DMF (0.6 mL), a catalytic amount of tetrakis(triphenylphosphine)palladium(0) [$Pd(PPh_3)_4$; 26 mg, 0.03 mmol] was added. The mixture was allowed to stir for 2 days at 110 °C. After reaction completion and cooling to room temperature, the mixture was poured into methanol (200 mL). The precipitated solid was recovered by filtration in a Soxhlet thimble and extracted with acetone, hexane, and chloroform for 12 h each. GPC (Chloroform, polystyrene standard, 25 °C): M_n = 71882, PDI = 3.2.

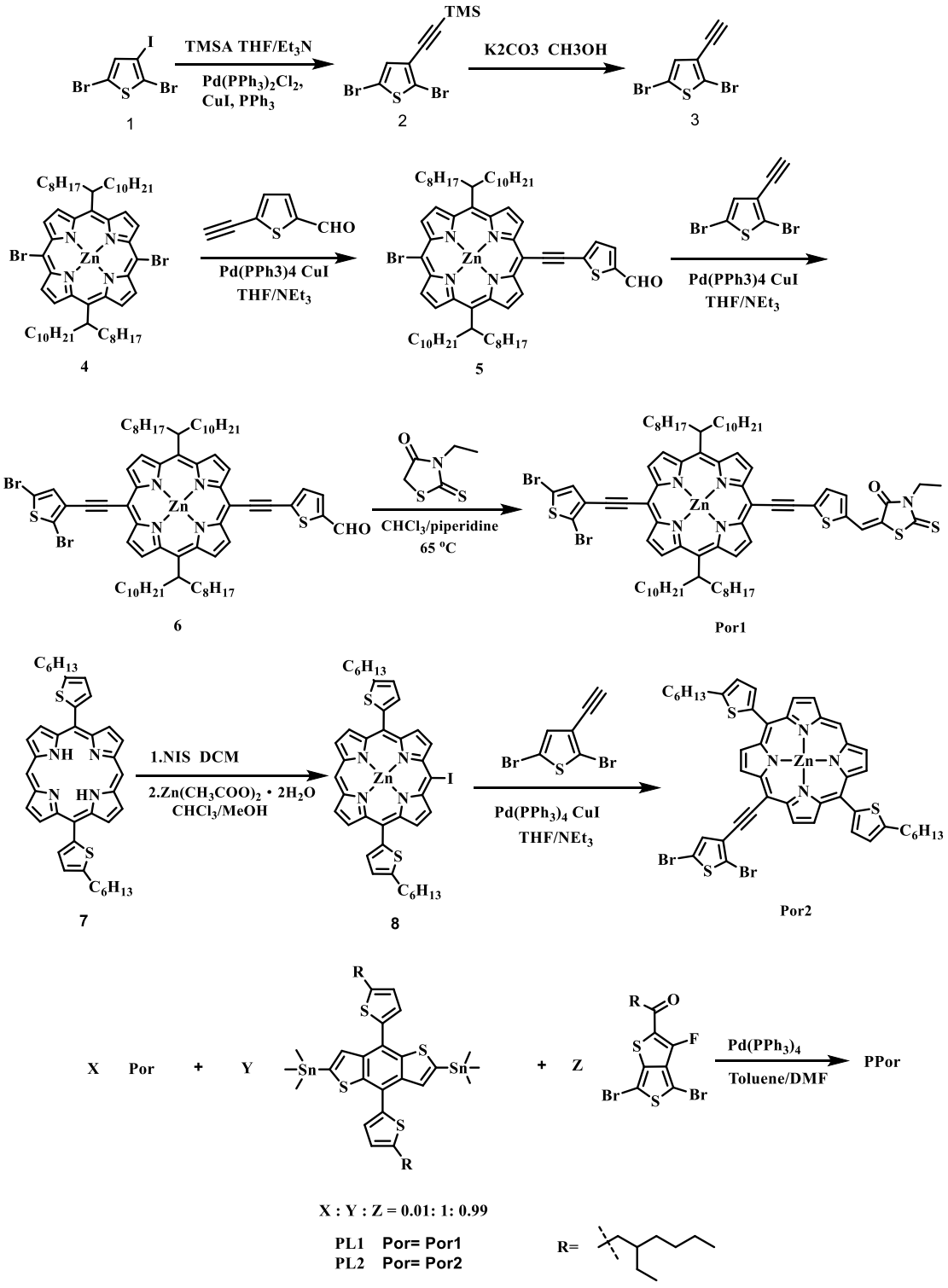

Scheme 1. Synthetic routes of **PL1** and **PL2**.

2.1.9. Synthesis of **PL2**

To an eggplant type reaction bottle containing compounds **4** (12.1 mg, 0.01 mmol), BDT (100 mg, 0.111 mmol) and TT (48.4 mg, 0.110 mmol) in a mixture of degassed toluene (2.4 mL) and DMF (0.6mL), a catalytic amount of tetrakis(triphenylphosphine)palladium(0) [$Pd(PPh_3)_4$; 26 mg, 0.03 mmol] was added. The mixture was allowed to stir for 2 days at 110 °C. After reaction completion and cooling to room temperature, the mixture was poured into methanol (200 mL). The precipitated solid was recovered by filtration in a Soxhlet thimble and extracted with acetone, hexane, and chloroform for 12 h each. GPC (THF, polystyrene standard, 25 ^oC): M_n = 112268, PDI = 2.32.

2.2 Instruments and characterization

NMR spectra were recorded on a Bruker AV400 MHz FTNMR spectrometer with TMS as the internal standard with deuterated chloroform as solvent at 25 °C. UV-vis spectra were recorded with a PE Lamda 25 UV-Vis spectrometer. Thermogravimetric analysis (TGA) measurements were conducted on a TA Q600 thermogravimetric analyzer under nitrogen at a heating rate of 20 °C min^{-1}. Cyclic voltammetry was performed using a CHI6600B workstation, and measurements were carried out in anhydrous acetonitrile containing 0.1 M Bu_4NPF_6 as a supporting electrolyte. Glassy carbon electrode coated with polymer film and platinum piece was used as a working electrode and a counter electrode respectively. Saturated calomel electrode served as a reference electrode, and the scan rate was 100 mV s^{-1}. The samples for testing were prepared from film using chloroform. The atomic force microscopy (AFM) measurements of the surface morphology of samples were conducted on a Dimension 3100 (Veeco) Atomic Force Microscope in the tapping mode.

2.3 Fabrication and characterization of solar cells

The photovoltaic devices with a conventional structure (as shown in **Figure 1**) of ITO/PEDOT:PSS/donor:$PC_{71}BM$/PFN/Al was constructed to evaluate the photovoltaic performance. All the active layers with or without 1.5% DIO additive were spin-cast from chlorobenzene solution (donor:acceptor = 1:1.5). The current-voltage (*J*–*V*) characteristics of the devices were measured on a Keithley 2450 Source Measure Unit. The current–voltage characteristics of the solar cells were measured under the illumination of AM 1.5G (100 mW/cm^2) using a SS-F5-3A (Enli Technology Co. Ltd.) solar simulator (AAA grade, 50 mm x 50 mm photobeam size). The EQE was measured by Solar Cell Spectral Response Measurement System QER3011 (Enli Technololy Co. Ltd.). The light intensity at each wavelength was calibrated with a standard single-crystal Si photovoltaic cell.

3. Results and Discussion

3.1 Synthesis and structure characterization

The synthetic routes for the monomers and polymers are illustrated in **Scheme 1**. The thiophene-substituted porphyrin center was synthesized through the Stille coupling reaction between 2,5-dibromo-3-ethynylthiophene and each of the compounds **5** and **8** using $Pd(PPh_3)_4$ and CuI as the catalyst for 24 h. The **PL1** and **PL2** were synthesized through the Stille coupling reaction and showed good solubility in common organic solvents such as chloroform and tetrahydrofuran. Gel permeation chromatography (GPC) was utilized to measure the molecular weight of the polymer. The number average molecular weights (M_n) of the polymers were 71.8 and 112.2 kDa for **PL1** and **PL2**, respectively, with polydispersity indexes (PDI) of 3.21 and 2.32. The thermal properties of the two polymers were studied by TGA and the results are shown in Figure S6. The TGA curves reveal that the decomposition

temperatures with 5% weight-loss (T_d) of **PL1** and **PL2** are 329 °C and 326 °C, respectively, which indicates that they have good thermal stability for the application in OPVs.

3.2. Photophysical characterization

Figure 2 and **Table 1** depict the absorption spectra and optical data of **PL1** and **PL2** measured in chloroform ($CHCl_3$) solution and in thin solid films, which showed the maximum absorption peak at 682 nm, and the shoulder peak at 639 nm, but the shoulder peak of **PL1** was more intense. Obviously, it shows that the aggregation of **PL1** is stronger in the solution state, but the absorption of porphyrin Soret band of **PL2** at 432 nm is more obvious than that of **PL1**. In the film state, the absorption of **PL1** and **PL2** is obviously red-shifted, the shoulder of **PL2** is enhanced, and the shoulder of **PL1** is weakened, indicating that **PL2** may have stronger π-electron delocalization and intermolecular π-π stacking. Perhaps it can cause a higher J_{sc}. The absorption edges (λ_{on}) of **PL1** and **PL2** are 816 nm and 761 nm, respectively, and the corresponding optical band gaps (E_g^{opt}) are 1.52 eV and 1.63 eV, respectively. The narrow band gap is favorable for the generation of excitons, which may bring about high J_{sc} and PCE.

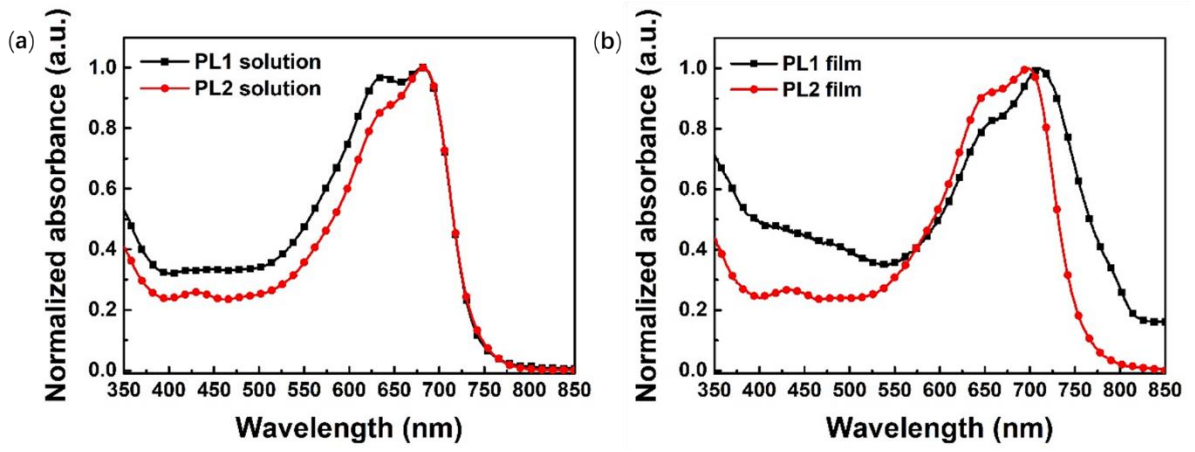

Figure 2. Absorption spectra of **PL1** and **PL2** in $CHCl_3$ solution (a) and in film (b)

Table 1. Optical and electrochemical properties for **PL1** and **PL2**.

Polymer	λ_{sol} (nm)	λ_{film} (nm)	λ_{on} (nm)	E_g^{opt} [a] (eV)	E_{ox}^{on} (V)	E_{red}^{on} (V)	HOMO[b] (eV)	LUMO[c] (eV)	E_g^{ec} [d] (eV)
PL1	639, 682	711	816	1.52	0.98	-0.80	-5.38	-3.60	1.78
PL2	639, 682	431, 698	761	1.63	1.04	-0.93	-5.44	-3.47	1.97

[a] $E_g^{opt} = 1240/\lambda_{on.}$ [b] HOMO = -(E_{ox}^{on} + 4.4). [c] LUMO = -(E_{red}^{on} + 4.4). [d] E_g^{ec} = LUMO-HOMO.

3.3 Electrochemical properties

In order to obtain the information of the frontier orbital energy levels of the two polymers, we investigated their redox behaviours by cyclic voltammetry (CV) in acetonitrile containing 0.10 mol L^{-1} tetrabutylammonium hexafluorophosphate (Bu_4NPF_6) as the supporting electrolyte and an Ag/Ag^+ electrode as the reference electrode (**Figure 3**). The energy levels (HOMO and LUMO) of the two polymers were calculated from the onset of the oxidation and reduction potentials by assuming the energy level of ferrocene/ferrocenium (Fc/Fc^+) to be -4.8 eV below the vacuum level. The formal potential of Fc/Fc^+ was measured as 0.40 V against Ag/Ag^+. The onset oxidation (E_{ox}^{on}) and reduction (E_{red}^{on}) potentials are 0.98 and -0.80 V, 1.04 and -0.93 V for **PL1** and **PL2**, respectively. According to the empirical equation, E_{HOMO} = -(E_{ox}^{on} + 4.4) (eV) and E_{LUMO} = -(E_{red}^{on} + 4.4) (eV), respectively, the corresponding HOMO and LUMO energies were estimated to be -5.38 and -3.60 eV, -5.44 and -3.47 eV for **PL1** and **PL2**, respectively. As compared with the HOMO (-6.0 eV) and LUMO (-4.19 eV) energy levels for $PC_{71}BM$, the polymer donors can have prominent exciton dissociation. The low HOMO levels of these two polymers facilitate the generation of high open circuit voltages in BHJ polymer solar cells.[34] Notably, the strategy of embedding a low ratio of porphyrin units to the D-A copolymer side chain as pendants can present fairly low-lying HOMO levels, as well as suitable band gaps (E_g), which guaranteed high V_{oc} of the OSCs when blended with $PC_{71}BM$, because V_{oc} is proportional to the energy difference between the LUMO of the acceptor and the HOMO of the donor.[35, 36]

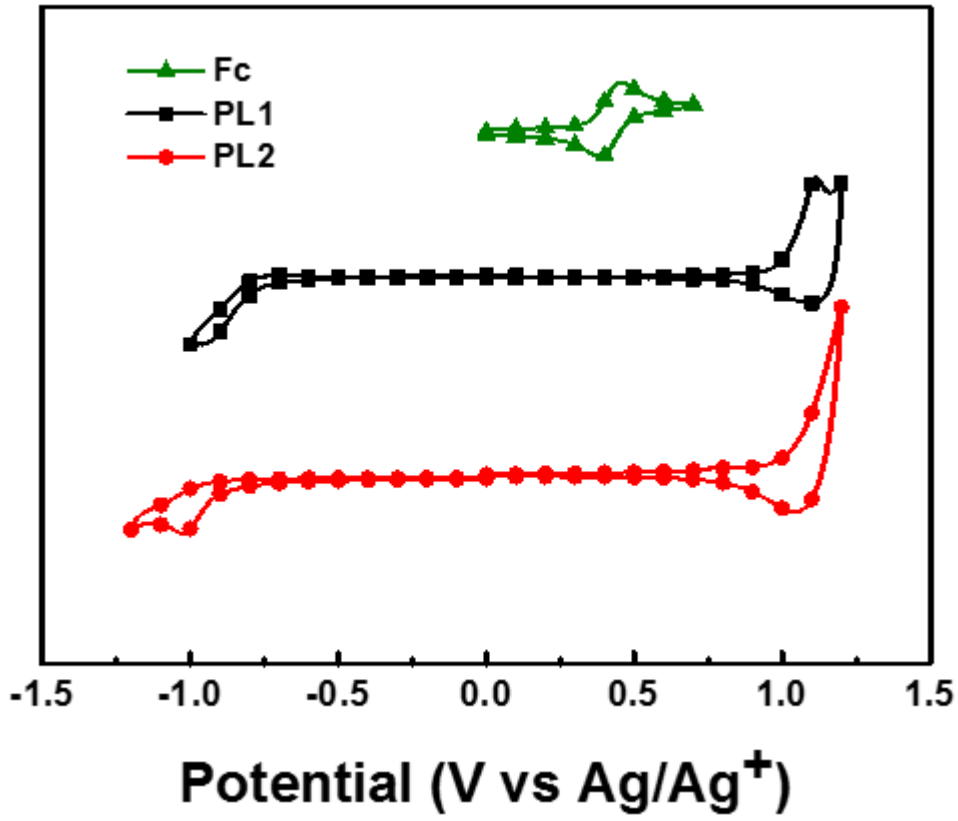

Figure 3. Cyclic voltammograms of the polymer films on a platinum electrode in 0.1 mol L^{-1} Bu_4NPF_6 in acetonitrile solution at a scan rate of 50 mV s^{-1}.

3.4 Photovoltaic properties

The photovoltaic properties of **PL1** and **PL2** were investigated with the solution-processed BHJ OSCs using $PC_{71}BM$ as the electron acceptor and two polymers as the electron donors under a conventional device structure of ITO/PEDOT:PSS/donor:$PC_{71}BM$/PFN/Al, and then measured under AM 1.5 G illumination. The ratio of polymer donor and $PC_{71}BM$ was optimized to be 1:1.5 (w/w) and those blend films were processed with 1.5% DIO additive from chlorobenzene. The current density-voltage (*J*–*V*) characteristics and external quantum efficiency (EQE) are shown in **Figure 4**, and the key device parameters are included in **Table 2**. As seen in Table 2, the devices without DIO additive based on **PL1** and **PL2** show low PCEs of only 3.90% and 4.00%, respectively. But with 1.5% DIO additive in the active layers, the PCEs are raised remarkably to 5.73% and 7.14%, respectively, contributed by the significantly improved J_{sc} and FF values, although the V_{oc} values are reduced slightly. The

decrease of V_{oc} but the increase of J_{sc} and FF values can be ascribed to the strengthened crystallinity of the porphyrins.[37, 38] It is also noted that among all those devices with 1.5% DIO or without DIO additive, the **PL2**-based devices show better PCEs with the higher J_{sc} and FF values than **PL1**, which can be partially attributed to the better intramolecular charge transfer (ICT) and better intermolecular π-π stacking of **PL2**.[39] As shown in **Figure 4b**, the external quantum efficiency (EQE) curves of the two optimized devices were measured, and all the devices show a very wide range of photocurrent generation in the region of 300 to 800 nm. The J_{sc} values are calculated to be 11.2 and 13.8 mA cm^{-2} for the devices based on **PL1** and **PL2**, respectively, which agree well with the measured values. It is worth noting that the overall EQE values of **PL1**-based device are relatively lower, leading to the lower J_{sc} value of 12.3 mA cm^{-2}, but the EQE values of **PL2**-based devices are higher from 428 nm to 800 nm, leading to the higher J_{sc} value of 15.2 mA cm^{-2}.

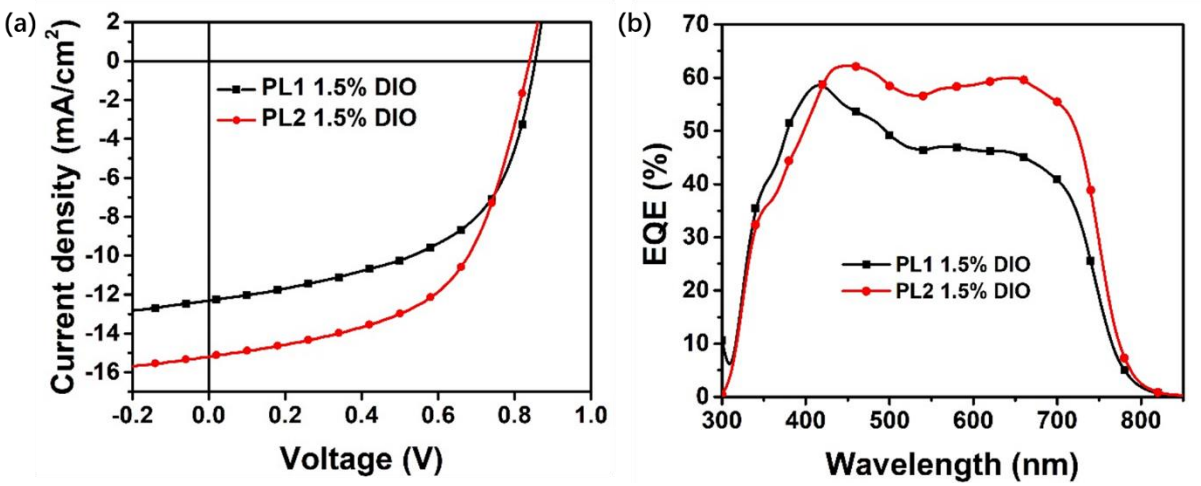

Figure 4. (a) *J*–*V* curves of the BHJ OSCs based on donor/$PC_{71}BM$ (1:1.5, with 1.5% DIO) under the illumination of AM 1.5 G at 100 mW cm^{-2}. (b) EQE curves of the devices based on donor/$PC_{71}BM$ (1:1.5, with 1.5% DIO)

Table 2. Photovoltaic properties of the OSCs based on donor/$PC_{71}BM$ (1:1.5, with 1.5% DIO) under the illumination of AM 1.5 G, 100 mW cm^{-2}.

Polymer	V_{oc} (V)	J_{sc}[c] (mA cm^{-2})	FF (%)	PCE[d] (%)	μ_h (cm^2 V^{-1} s^{-1})	μ_e (cm^2 V^{-1} s^{-1})
PL1[a]	0.95	9.05	45.5	3.90 (3.81)	1.90×10^{-4}	1.26×10^{-4}
PL1[b]	0.86	12.3 (11.2)	54.4	5.73 (5.57)	8.94×10^{-4}	4.56×10^{-4}
PL2[a]	0.95	9.25	45.4	4.00 (3.92)	3.30×10^{-4}	2.43×10^{-4}
PL2[b]	0.84	15.2 (13.8)	55.9	7.14 (7.03)	1.01×10^{-3}	8.95×10^{-4}

[a] As-cast devices. [b] With DIO (1.5%, v/v) as additive. [c] Values calculated from EQE in brackets. [d] Average value for 20 same devices in brackets.

3.5. Charge transport mobility

A space charge-limited current (SCLC) model was used to estimate the charge carrier mobility of the blend films. We have measured the hole and electron mobilities of the two donor/$PC_{71}BM$ blend films from the *J–V* characteristics of the hole only and electron only devices in dark. The information on the charge transfer properties of the fitted curve in the space charge limiting current (SCLC) model and the values are shown in **Figure 5**, Figure S8 and **Table 2**. Obviously, the device based on the material with a larger hole mobility value shows a higher photovoltaic efficiency. All of the $P_{71}CBM$-based blend films exhibit balanced μ_h/μ_e ratios, which are beneficial to obtaining high FF values. Moreover, the μ_h/μ_e values of **PL1** and **PL2** with 1.5% DIO are 1.96 and 1.13, respectively. The device based on **PL2** has a better hole/electron balance than **PL1**-based device, leading to less charge recombination and higher J_{sc} and FF values of the OSC.[40] The carrier recombination behaviors of the solar cells were investigated by measuring the dependence of J_{sc} and V_{oc} on the intensity of incident light (P_{light}). The photovoltaic devices with 1.5% DIO additive based on these two polymers, J_{sc} under different light intensities (P) were measured, and its relationship with P can be expressed as $J_{sc} \propto P^{\alpha}$, where α is an exponential factor.[41] Ideally, the carriers can be completely collected by the two poles before recombination, and the relationship coefficient α should be 1 in this case. In general, the higher α value (α<1) represents less bimolecular

recombination. On the other hand, when α>1, there is recombination of defects.[42] As shown in Figure S9, the values of α for the **PL1**- and **PL2**-based devices are 0.893 and 0.991, respectively, indicating that there is only bimolecular recombination, but the value of α for **PL2**-based device is closer to 1, meaning that the recombination of **PL2**-based device is less, which is consistent with its higher J_{sc} and FF.

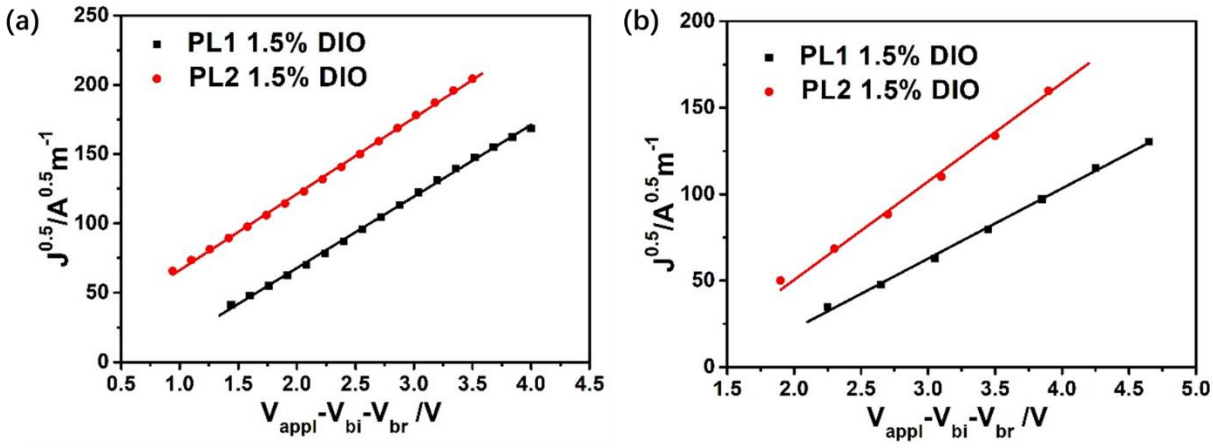

Figure 5. $J^{0.5}$ *vs* V_{appl} curves of the hole-only (a) and electron-only (b) devices according to the SCLC method.

3.6 Film morphology

The morphologies of the blend films were investigated by atomic force microscopy in the tapping mode (**Figure 6**). As seen in the AFM images, the morphology of polymer: $PC_{71}BM$-based BHJ thin films spin-coated without and with 1.5% DIO additive exhibits different surfaces. The root-mean-square (RMS) of the blend films based on **PL1** and **PL2** are 0.31 nm and 0.37 nm, respectively. They show higher RMS roughness values (0.78 nm and 0.74 nm, respectively.) after adding 1.5% DIO, indicating optimized nanoscale phase separation and bicontinuous D/A interpenetrating network structure, which could facilitate the separation of excitons in the composite films, thereby contributing to the improvement of J_{sc} and FF as well as a greater mobility.

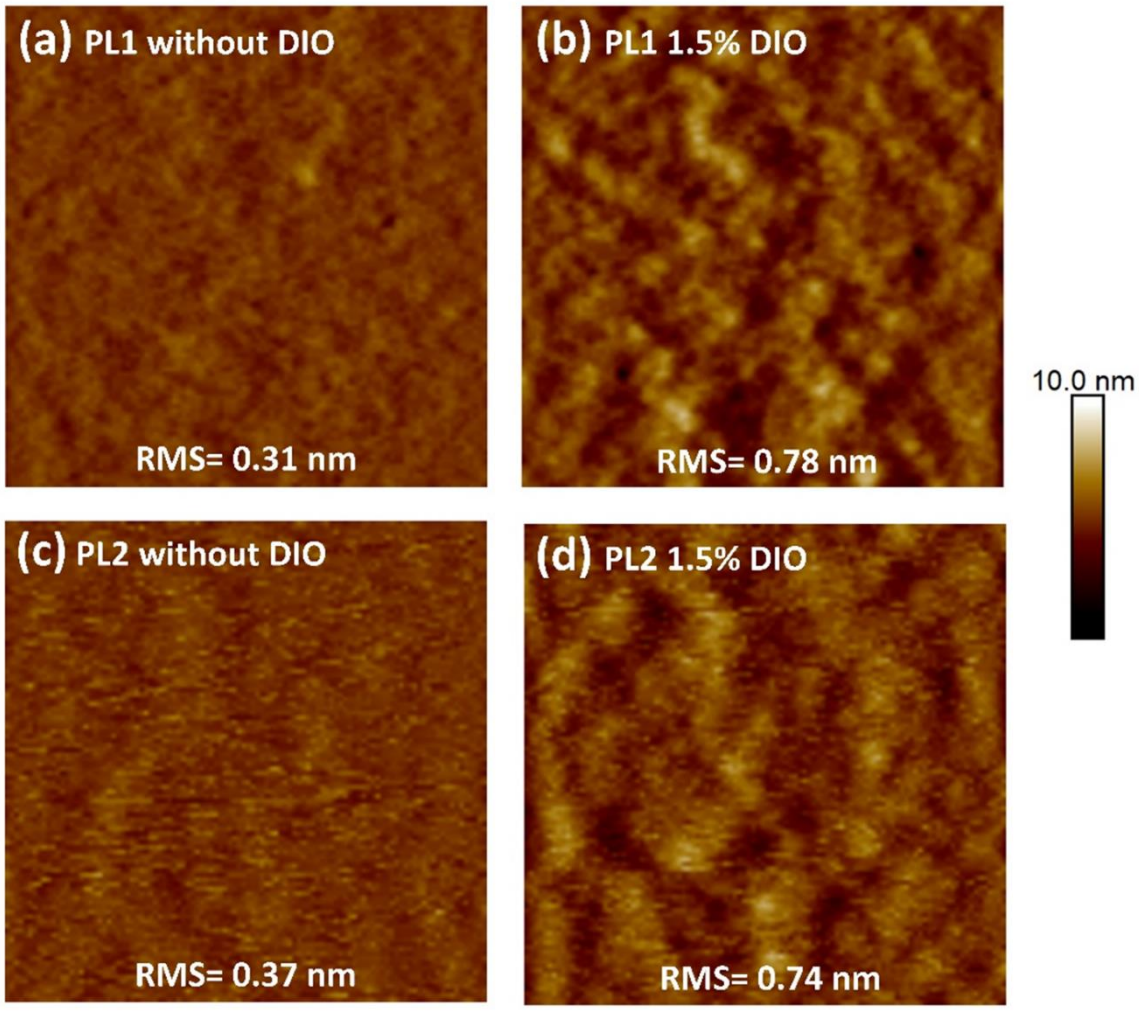

Figure 6. (a), (b), (c) and (d) AFM height images (1 × 1 μm, tapping-mode) of **PL1**/$PC_{71}BM$, **PL2**/$PC_{71}BM$, **PL1**/$PC_{71}BM$ with 1.5%DIO and **PPor-II**/$PC_{71}BM$ with 1.5% DIO composite film, respectively.

4. Conclusions

In summary, two new block copolymers with porphyrin-incorporated side chains as pendants were designed and synthesized. They have good solubility in common organic solvents, and the introduction of porphyrin units renders them panchromatic absorbers. Films with 1.5% DIO addtive based on **PL1** as donor afforded 5.73% photoelectric conversion efficiency. When the porphyrin pendant is shrinked properly, a 7.14% efficiency was obtained from **PL2**-based blend films with higher J_{sc} and FF, more balanced carrier mobility, less bimolecular

recombination and better blend morphology. These results indicate that the strategy, in which a conventional D-A polymer side chain is embedded with a porphyrin pendant, is effective to realize high-performance solution-processed BHJ OSCs. The size of the porphyrin pendant affects the optical properties and electrochemical properties of the polymer. By adjusting the size of the porphyrin pendant appropriately, the charge transport and film morphology of the device can be effectively improved, which further benefits the development of high performance copolymers for OSCs with well-matched acceptors and/or donors materials.

Supporting Information

Supporting Information is available from the Wiley Online Library or from the author.

Acknowledgements:

Z. Liu and Z. Huang contributed equally to this work. This work was supported by the National Natural Science Foundation of China (Grant Nos. 51473139, 51573120 and 51773142), the Natural Science Foundation of Hunan Province (Grant No.2019JJ50603), Graduate student scientific research innovation projects in Hunan province (Grant Nos. CX2018B368 and CX2017B303), the Innovation Platform Open Foundation of University of Hunan Province (Grant No.14K092) and Hunan 2011 Collaborative Innovation Center of Chemical Engineering & Technology with Environmental Benignity and Effective Resource Utilization. S. Hu thanks the Xiangtan University Undergraduate Innovative Experiment Program. W.-Y. W. thanks the financial support from the Science, Technology and Innovation Committee of Shenzhen Municipality (JCYJ20170303160036674), Hong Kong Research Grants Council (PolyU123384/16P), the Areas of Excellence Scheme, University Grants Committee, HKSAR (AoE/P-03/08), Hong Kong Polytechnic University (1-ZE1C) and the Endowed Professorship in Energy from Ms. Clarea Au (847S).

Conflict of Interest

The authors declare no conflict of interest.

Received: Month XX, XXXX; Revised: Month XX, XXXX; Published online:

DOI: 10.1002/marc

Keywords

polymer solar cells; block copolymers; bulk heterojunction; porphyrin; organic photovoltaics

[1] R. F. Service, *Science (New York, NY)* **2011**, *332*, 293.

[2] L. Lu, T. Zheng, Q. Wu, A. M. Schneider, D. Zhao, L. Yu, *Chem. Rev.* **2015**, *115*, 12666.

[3] W.-Y. Wong, X.-Z. Wang, Z. He, A. B. Djurišić, C.-T. Yip, K.-Y. Cheung, H. Wang, C. S. Mak, W.-K. Chan, *Nat. Mater.* **2007**, *6*, 521.

[4] W.-Y. Wong, X.-Z. Wang, Z. He, K.-K. Chan, A. B. Djurišić, K.-Y. Cheung, C.-T. Yip, A. M.-C. Ng, Y. Y. Xi, C. S. Mak, *J. Am. Chem. Soc.* **2007**, *129*, 14372.

[5] D. Ye, X. Li, L. Yan, W. Zhang, Z. Hu, Y. Liang, J. Fang, W.-Y. Wong, X. Wang, *J. Mater. Chem. A* **2013**, *1*, 7622.

[6] H. Wang, L. Xiao, L. Yan, S. Chen, X. Zhu, X. Peng, X. Wang, W.-K. Wong, W.-Y. Wong, *Chem. Sci.* **2016**, *7*, 4301.

[7] J. Zhao, Y. Li, G. Yang, K. Jiang, H. Lin, H. Ade, W. Ma, H. Yan, *Nat. Energy* **2016**, *1*, 15027.

[8] Y. J. You, C. E. Song, Q. V. Hoang, Y. Kang, J. S. Goo, D. H. Ko, J. J. Lee, W. S. Shin, J. W. Shim, *Adv. Funct. Mater.* **2019**, 1901171.

[9] Z.-G. Zhang, Y. Li, *Sci. China Chem.* **2015**, *58*, 192.

[10] X. Xu, T. Yu, Z. Bi, W. Ma, Y. Li, Q. Peng, *Adv. Mater.* **2018**, *30*, 1703973.

[11] Q. Fan, W. Su, Y. Wang, B. Guo, Y. Jiang, X. Guo, F. Liu, T. P. Russell, M. Zhang, Y. Li, *Sci. China Chem.* **2018**, *61*, 531.

[12]B. Kan, H. Feng, H. Yao, M. Chang, X. Wan, C. Li, J. Hou, Y. Chen, *Sci. China Chem.* **2018**, *61*, 1307.

[13]J. Yuan, Y. Zhang, L. Zhou, G. Zhang, H.-L. Yip, T.-K. Lau, X. Lu, C. Zhu, H. Peng, P. A. Johnson, *Joule* **2019**, *3*, 1140.

[14]K. Jiang, Q. Wei, J. Y. L. Lai, Z. Peng, H. K. Kim, J. Yuan, L. Ye, H. Ade, Y. Zou, H. Yan, *Joule* **2019**.

[15]X. Xu, K. Feng, Z. Bi, W. Ma, G. Zhang, Q. Peng, *Adv. Mater.* **2019**, 1901872.

[16]H. Hayashi, W. Nihashi, T. Umeyama, Y. Matano, S. Seki, Y. Shimizu, H. Imahori, *J. Am. Chem. Soc.* **2011**, *133*, 10736.

[17] S. Mathew, A. Yella, P. Gao, R. Humphry-Baker, B. F. Curchod, N. Ashari-Astani, I. Tavernelli, U. Rothlisberger, M. K. Nazeeruddin, M. Grätzel, *Nat. Chem.* **2014**, *6*, 242.

[18] W. M. Campbell, K. W. Jolley, P. Wagner, K. Wagner, P. J. Walsh, K. C. Gordon, L. Schmidt-Mende, M. K. Nazeeruddin, Q. Wang, M. Grätzel, *J. Phys. Chem. C* **2007**, *111*, 11760.

[19] T. Bessho, S. M. Zakeeruddin, C. Y. Yeh, E. W. G. Diau, M. Grätzel, *Angew. Chem. Int. Ed.* **2010**, *49*, 6646.

[20] S. Chen, L. Yan, L. Xiao, K. Gao, W. Tang, C. Wang, C. Zhu, X. Wang, F. Liu, X. Peng, *J. Mater. Chem. A* **2017**, *5*, 25460.

[21] X. Zhou, W. Tang, P. Bi, L. Yan, X. Wang, W.-K. Wong, X. Hao, B. S. Ong, X. Zhu, *J. Mater. Chem. A* **2018**, *6*, 14675.

[22] X. Zhou, W. Tang, P. Bi, Z. Liu, W. Lu, X. Wang, X. Hao, W.-K. Wong, X. Zhu, *J. Mater. Chem. C* **2019**, *7*, 380.

[23] J. Kesters, P. Verstappen, M. Kelchtermans, L. Lutsen, D. Vanderzande, W. Maes, *Adv. Energy Mater.* **2015**, *5*.

[24] C.-L. Mai, W.-K. Huang, H.-P. Lu, C.-W. Lee, C.-L. Chiu, Y.-R. Liang, E. W.-G. Diau, C.-Y. Yeh, *Chem. Commun.* **2010**, *46*, 809.

[25] J. Hatano, N. Obata, S. Yamaguchi, T. Yasuda, Y. Matsuo, *J. Mater. Chem.* **2012**, *22*, 19258.

[26] L.-L. Li, E. W.-G. Diau, *Chem. Soc. Rev.* **2013**, *42*, 291.

[27] Z. S. Wang, W. E. Sha, W. C. Choy, *J. Appl. Phys.* **2016**, *120*, 213101.

[28] F. He, L. Yu, *J. Phys. Chem. Lett.* **2011**, *2*, 3102.

[29] Y. H. Chao, J. F. Jheng, J. S. Wu, K. Y. Wu, H. H. Peng, M. C. Tsai, C. L. Wang, Y. N. Hsiao, C. L. Wang, C. Y. Lin, *Adv. Mater.* **2014**, *26*, 5205.

[30] C.-H. Li, C.-C. Chang, Y.-H. Hsiao, S.-H. Peng, Y.-J. Su, S.-w. Heo, K. Tajima, M.-C. Tsai, C.-Y. Lin, C.-S. Hsu, *ACS Appl. Mater. Interfaces* **2018**, *11*, 1156.

[31] T. Ameri, G. Dennler, C. Lungenschmied, C. J. Brabec, *Energy Environ. Sci.* **2009**, *2*, 347.

[32] H. Zhou, Y. Zhang, C. K. Mai, S. D. Collins, T. Q. Nguyen, G. C. Bazan, A. J. Heeger, *Adv. Mater.* **2014**, *26*, 780.

[33] K. Gao, J. Miao, L. Xiao, W. Deng, Y. Kan, T. Liang, C. Wang, F. Huang, J. Peng, Y. Cao, *Adv. Mater.* **2016**, *28*, 4727.

[34] Z. Li, G. He, X. Wan, Y. Liu, J. Zhou, G. Long, Y. Zuo, M. Zhang, Y. Chen, *Adv. Energy Mater.* **2012**, *2*, 74.

[35] Y. Li, Q. Guo, Z. Li, J. Pei, W. Tian, *Energy Environ. Sci.* **2010**, *3*, 1427.

[36] H.-Y. Chen, J. Hou, S. Zhang, Y. Liang, G. Yang, Y. Yang, L. Yu, Y. Wu, G. Li, *Nat. Photonics* **2009**, *3*, 649.

[37] C. V. Kumar, L. Cabau, E. N. Koukaras, G. D. Sharma, E. Palomares, *Nanoscale* **2015**, *7*, 179.

[38] C. V. Kumar, L. Cabau, E. N. Koukaras, A. Sharma, G. D. Sharma, E. Palomares, *J. Mater. Chem. A* **2015**, *3*, 16287.

[39] J. Hou, H.-Y. Chen, S. Zhang, G. Li, Y. Yang, *J. Am. Chem. Soc.* **2008**, *130*, 16144.

[40] J. Zhang, Y. Zhang, J. Fang, K. Lu, Z. Wang, W. Ma, Z. Wei, *J. Am. Chem. Soc.* **2015**, *137*, 8176.

[41] L. Koster, V. Mihailetchi, H. Xie, P. Blom, *Appl. Phys. Lett.* **2005**, *87*, 203502.

[42] S. R. Cowan, A. Roy, A. J. Heeger, *Phys. Rev. B* **2010**, *82*, 245207.

.

Graphical Abstract

Two new block copolymers with porphyrin-incorporated side chains as pendants were synthesized. Such strategy, in which a conventional D-A polymer side chain is embedded with a porphyrin pendant, is effective to realize high-performance solution-processed bulk-heterojunction organic solar cells.